



HAL
open science

A comprehensive study of the spatial distribution of the galvanic protection current supplied by zinc layer anodes applied to steel-reinforced concrete structures

David Garcia, S. Laurens, S. Panin

► To cite this version:

David Garcia, S. Laurens, S. Panin. A comprehensive study of the spatial distribution of the galvanic protection current supplied by zinc layer anodes applied to steel-reinforced concrete structures. *Corrosion Science*, 2019, 158, pp.108108. 10.1016/j.corsci.2019.108108 . hal-02310676

HAL Id: hal-02310676

<https://hal.insa-toulouse.fr/hal-02310676>

Submitted on 20 Dec 2021

HAL is a multi-disciplinary open access archive for the deposit and dissemination of scientific research documents, whether they are published or not. The documents may come from teaching and research institutions in France or abroad, or from public or private research centers.

L'archive ouverte pluridisciplinaire **HAL**, est destinée au dépôt et à la diffusion de documents scientifiques de niveau recherche, publiés ou non, émanant des établissements d'enseignement et de recherche français ou étrangers, des laboratoires publics ou privés.



Distributed under a Creative Commons Attribution - NonCommercial 4.0 International License

1 **A comprehensive study of the spatial distribution of the galvanic**
2 **protection current supplied by zinc layer anodes applied to steel-**
3 **reinforced concrete structures**

4
5 **D. Garcia**¹, **S. Laurens**^{1,*}, **S. Panin**²

6
7 ^a Université de Toulouse, UPS, INSA, LMDC 135 avenue de Rangueil 31077 Toulouse Cedex 4 France

8 ^b R3S, N°18 ZA Les Pignès, 09270 Mazères France

9

10 Corresponding author: stephane.laurens@insa-toulouse.fr

11

12 **Abstract**

13

14 Improving the design of cathodic protection systems applied to steel-reinforced concrete structures
15 requires a comprehensive description of the on-going physical phenomena in order to achieve robust
16 engineering models. In this context, this paper deals with one highly relevant question of cathodic
17 protection design: the spatial distribution of the protecting current over the reinforcing steel. The issue
18 is addressed here, for the specific case of zinc layer anodes, by means of experimental tests performed
19 on simple laboratory specimens, together with numerical simulations resulting from theoretical
20 analysis of the physical problem. Particular attention is given to oxygen availability and concrete
21 moisture.

22

23 **Keywords:** Steel reinforced concrete – Cathodic protection – Modelling – Oxygen supply —

24 Numerical simulation

25

26 1 Introduction

27

28 It is well known that steel corrosion leads to accelerated deterioration of reinforced concrete
29 structures. Due to the high alkalinity of the concrete pore solution, a thin, compact and stable passive
30 oxide layer is formed on the steel surface. This phenomenon is referred to as steel passivation, which
31 actually corresponds to a uniform corrosion state, but with negligible corrosion rates. The local
32 dissolution of the passive film induced by partial carbonation of the concrete cover or local high
33 chloride concentration generates the condition of macrocell (or localized) corrosion. In other words,
34 when an active (depassivated) steel area is formed, its corrosion rate is significantly increased by
35 galvanic exchanges with the surrounding passive steel. In addition to structural problems resulting
36 from steel section losses, corrosion-induced rust expansion may cause other severe damage to RC
37 structures, such as concrete cover cracking, spalling and delamination [1].

38 In this context, the implementation of cathodic protection (CP) in RC structures has grown
39 substantially during the past two decades. Several design standards have been proposed for cathodic
40 protection, such as the NACE SP0216 and SP0290 [2] or the EN 12696 standard [3]. Generally
41 speaking, CP design and performance criteria, as well as monitoring methods, are based on empirical
42 assumptions that do not allow for optimization of the protection system. Therefore, improving the
43 design and control of CP systems requires a comprehensive description of on-going physical
44 phenomena from the scientific community in order to achieve robust engineering models [4], [5].

45 The corrosion of steel in concrete is an electrochemical process in which the dissolution of steel
46 constitutes the anodic reaction (Eq. 1), which provides electrons that are consumed by the cathodic
47 reaction corresponding to the reduction of oxygen dissolved in the interstitial solution of the concrete
48 (Eq. 2).



49 Two main types of steel corrosion are usually associated with reinforced concrete structures:

- 50 • Microcell corrosion: anodic and cathodic areas are immediately adjacent along the reinforcing
51 bar; each electron produced by steel dissolution is consumed locally by oxygen reduction
52 involving a negligible ohmic drop between anodic and cathodic areas. Both anodic and
53 cathodic areas reach the same electrochemical potential (E_{corr}), the global potential field is
54 uniform in the concrete volume and, consequently, no ionic current is produced.
55
- 56 • Macrocell (or galvanic) corrosion: anodic and cathodic areas at the steel-concrete interface are
57 spatially separated, so there is an electrolytic resistance between them. Therefore, anodic and
58 cathodic half-cells do not reach the same potential, resulting in a potential gradient and a
59 galvanic corrosion current in the concrete volume.

60 Actually, only uniform passive steel can be regarded as a uniform corrosion system in reinforced
61 concrete structures. Any other corrosion system, involving both active and passive steel areas, has to
62 be considered as a macrocell (or galvanic) system. It must be added that, whatever the environmental
63 exposure, steel bars in concrete cannot be uniformly depassivated, which means that a uniform active
64 state is not likely to occur. Obviously, a long-term galvanic process could lead to generalized

65 corrosion by growth and coalescence of active areas, but such a case is associated with very advanced
66 deterioration of the structure.

67 The theoretical concepts exposed above for steel corrosion can be extended to galvanic protection.
68 A galvanic protection is actually a macrocell corrosion system in which the natural oxidation of zinc,
69 connected to the reinforcing steel network, provides electrons consumed by oxygen reduction
70 primarily at the passive steel-concrete interface. Connecting zinc anodes to reinforcing bars in
71 concrete results in their mutual polarization. Since zinc in concrete is characterized by a modest
72 electrochemical potential of about -1000 mV vs SCE [6], passive and active steel areas are subjected
73 to cathodic polarization and zinc anodes undergo anodic polarization. Therefore, the macrocell
74 corrosion current between active and passive steel areas is mitigated, or may even be annihilated if the
75 galvanic protection system is correctly designed.

76 Physically, galvanic protection applied to corroding steel in concrete can be seen as a three-
77 component system: galvanic anode + active steel + passive steel. Compared to the pre-existing
78 macrocell system formed by active and passive steel areas, an additional macrocell current flows from
79 the sacrificial anode towards the reinforcing steel bars when they are connected. The potential gradient
80 in the concrete volume is also modified by the connection of this third component and the whole
81 system reaches a new electrochemical equilibrium.

82 The equilibrium achieved is defined by the rates of electrochemical reactions at the different
83 interfaces, the associated ionic current, and the potential field in the concrete volume. The equilibrium
84 is controlled by three predominant influencing factors:

- 85 • the respective electrochemical behaviours of the three components; this is referred to as charge
86 transfer control;
- 87 • the field of electrical resistivity in the concrete volume;
- 88 • the oxygen supply by diffusion through the partially-saturated concrete matrix towards the
89 cathodic regions at the steel-concrete interface; this is referred to as mass transfer control.

90 According to Raupach [7], the degree of pore water saturation in the cementitious matrix and its
91 influence on oxygen diffusion properties are key parameters for modelling the electrochemical process
92 occurring in reinforcement corrosion. Moreover, the saturation degree of concrete is the main
93 influencing factor of electrical resistivity. Both steel corrosion and cathodic protection in reinforced
94 concrete are highly dependent on oxygen diffusion and concrete resistivity but there is some
95 competition between these influencing factors. A dry concrete facilitates the oxygen supply (by
96 oxygen diffusion in the gaseous phase) but it is also associated with high electrical resistivity due to a
97 continuity breakdown in the liquid phase of the cementitious pore network and limiting galvanic
98 exchanges. Therefore, in dry concrete, corrosion and cathodic protection are controlled by electrical
99 and electrochemical phenomena, since oxygen supply is not a limiting factor. Conversely, in a water-
100 saturated concrete, the transport of dissolved oxygen in water filled pores is very slow, while the
101 electrolytic conductivity is very high [8]. In this case, galvanic exchanges are not controlled by
102 electrical resistivity but by the rate of the cathodic reaction, which is limited by the rate of oxygen
103 diffusion towards the steel reinforcements.

104 In the literature, the saturation value of cathodic current is introduced as the limiting current of
105 oxygen reduction (i_{lim}). This current may be simply deduced from Fick's first law (mass transport)
106 and Faraday's constant (electrochemistry) as follows:

$$J_{O_2} = -D_e \nabla c \quad (3)$$

$$i_{lim} = -4F J_{O_2} \quad (4)$$

107 where:

108 - J_{O_2} is the oxygen flux flowing through steel-concrete interface ($mol.m^{-2}.s^{-1}$),

109 - c is the local oxygen concentration ($mol.m^{-3}$),

110 - D_e is the effective diffusion coefficient of oxygen ($m^2.s^{-1}$),

111 - F is the Faraday constant ($= 96485 C.mol^{-1}$).

112 Several authors consider the oxygen diffusion as a one-dimensional problem with total
113 consumption of oxygen at the steel-concrete interface to simplify the estimation of concentration
114 gradient in the limiting current expression. However, these assumptions are only justified in fully
115 saturated concrete involving a linear concentration distribution through concrete cover. In partly
116 saturated concrete, the limiting current of oxygen reduction may be evaluated locally by using
117 appropriate 3D numerical methods to assess the concentration distribution in the concrete volume.
118 Therefore, the global electrochemical equilibrium relative to a galvanic protection system is a three-
119 dimensional non-linear physical problem. Computing such a 3D equilibrium requires the development
120 of appropriate numerical models [9], [10].

121 Electrochemical modelling and numerical simulation of cathodic protection implemented in RC
122 structures is a relatively recent research field. A few research works can be found on the numerical
123 simulation of coupled effects of the electrochemical process and oxygen diffusion through partly
124 saturated concrete to describe a corroding system [11]. However, the literature is very scarce regarding
125 the response of macrocell corrosion systems under cathodic polarization. This topic is nevertheless of
126 major importance regarding the aim of optimizing the design of cathodic protection in RC structures.

127 In a robust computational model of steel corrosion in concrete and/or a related cathodic protection
128 system, the three main influencing phenomena described above have to be taken into consideration to
129 provide realistic numerical simulations and to assess the cathodic polarization level of the reinforcing
130 network [8]:

- 131 • Electrochemical processes at the different metal-concrete interfaces: active steel/concrete,
132 passive steel/concrete, CP anodic system/concrete (such as zinc/concrete);
- 133 • Oxygen diffusion correlated to capillary water transport in the cementitious matrix;
- 134 • The field of electrical resistivity, which is also directly influenced by water transport.

135 In the work presented here, the specific case of galvanic protection by means of zinc layer anodes
136 (ZLA) was studied giving special attention to the impact of oxygen supply on the global macrocell
137 equilibrium. The spatial distribution of the protecting current from the galvanic anode towards the
138 steel reinforcement and the potential field was studied in relation with oxygen availability in the
139 concrete volume. Section 2 of this paper presents original experiments carried out to demonstrate the
140 relevance of oxygen availability as a predominant influencing factor of galvanic cathodic protection.
141 In section 3, the theoretical background necessary to achieve effective numerical simulations is
142 reported. Section 4 demonstrates the robustness of the numerical simulations by comparing them with
143 the experiments described in section 2.

144 2 Experimental investigations on concrete specimens

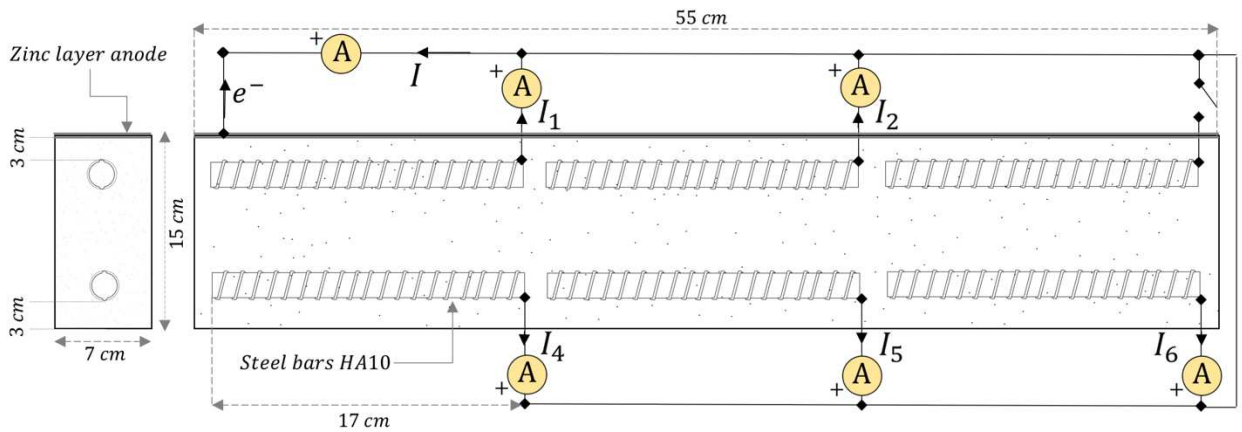
145

146 2.1 Experimental protocol

147

148 The following section presents some experiments specifically designed to highlight the relevance
149 of taking the oxygen supply into account as a predominant control parameter in the design of galvanic
150 protection systems. Experiments were carried out on a small concrete beam (Fig.1) in which six bars
151 were embedded in two layers: 3 upper steel bars (labelled 1 to 3) and three lower steel bars (labelled 4
152 to 6). The dimensions of the concrete slab were $55 \times 7 \times 15 \text{ cm}^3$. All steel bars were 1 cm in
153 diameter and 17 cm high. The concrete cover above the upper steel layer was 3 cm, while the lower
154 steel layer depth was 11 cm from the top side of the bars to the top concrete surface. The concrete mix
155 proportions were as follows: a water-cement ratio of 0.6, an aggregate-cement ratio of 2.8 and a sand-
156 cement ratio of 2.0. Curing consisted of covering the specimen with plastic sheathing for 7 days. The
157 zinc sheet backed with an ion conductive adhesive paste (ZLA) was applied to the top surface of the
158 specimen.

159 All the bars were independent, but welded metallic wires allowed for any electrical connection
160 between two or more steel bars, making it possible to generate different macrocell systems. In the
161 following experiments, all the steel bars were connected, except for bar 3, as shown in Fig.1. Bar 3 of
162 the upper layer was voluntarily unconnected in order to cause some non-uniformity of the polarization
163 field due to the asymmetric reinforcing network. In particular, the unconnected bar 3 did not produce
164 any masking effect on the protection current in this configuration.



165

166 Fig. 1 Experimental specimen: small concrete beam in dry condition (easy oxygen transport) embedding 6 independent
167 passive steel rods (test1)

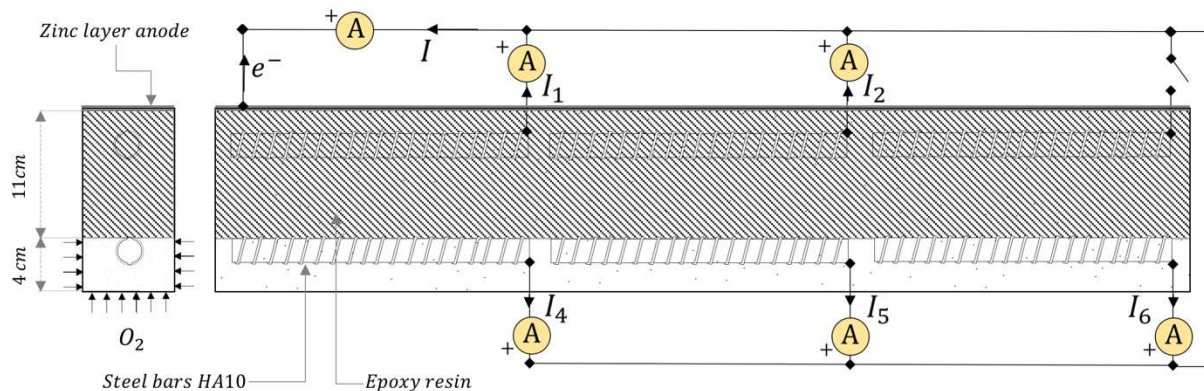
168 The bar output currents (I_1, I_2, I_4, I_5, I_6) were collected separately using a BioLogic® VMP3
169 multi-channel potentiostat-galvanostat. The ZRA technique was used to record the current flowing
170 between the working electrode (zinc layer anode) and each steel bar. This protocol enabled the spatial
171 distribution of the protection current supplied by the ZLA sheet over the 5 connected steel rods to be
172 reliably assessed.

173 Numerous tests were conducted on this specimen to compare numerical and experimental results
174 and to confirm experimental observations on various systems. For the whole duration of the tests, the

175 reinforcing network was kept in a passive electrochemical state. However, only two of the most
176 typical results summarizing experimental observations are presented below.

177 These experiments collected the protection current received by each of the five passive steel bars
178 embedded in a concrete slab under two different environmental conditions:

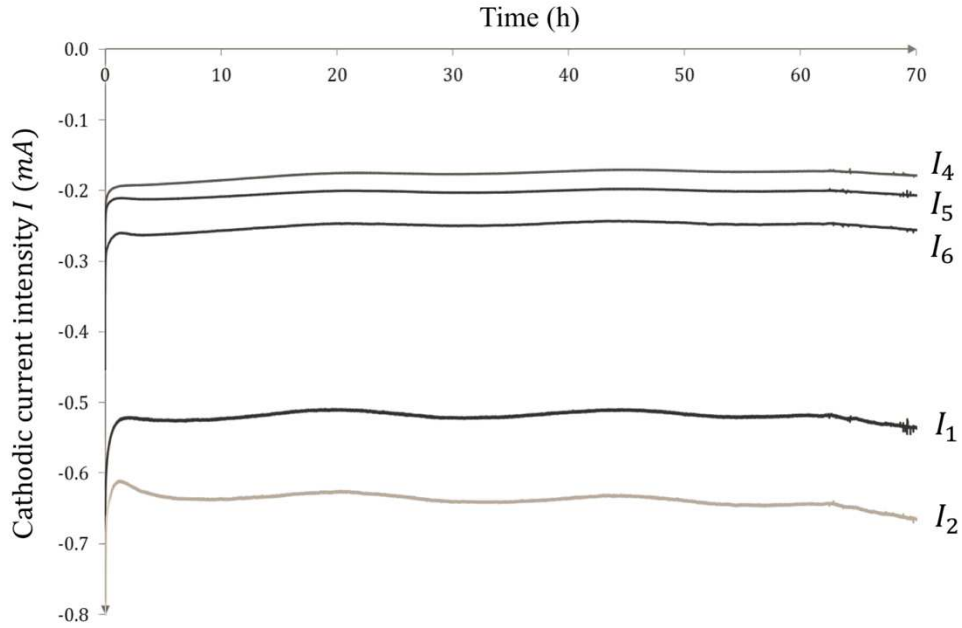
- 179 • **Test 1:** a concrete beam at hydric equilibrium in an air-conditioned room (Fig.1), involving a
180 fairly uniform moisture saturation degree of about 60 % (measured on small concrete test
181 cylinders coming from the same concrete mix). In such environmental conditions, oxygen
182 could be easily transported by diffusion towards all the steel rods in the concrete beam.
183
- 184 • **Test 2:** a partially coated concrete beam with fully moisture saturated concrete around the
185 upper steel bars (Fig. 2). The concrete beam was first immersed in tap water until its mass
186 stabilized. Then, an epoxy resin was applied to the upper part of the beam surface in order to
187 prevent oxygen diffusion to the upper steel layer. Gas transport through the cementitious
188 matrix was only allowed through the lower part of the beam, meaning that the lower steel
189 layer received much more oxygen than the upper layer. The water saturation field in the
190 concrete volume is not directly measurable but, since the resin coating also avoided any drying
191 process in the upper part of the beam, it can reasonably be considered that concrete was fully
192 saturated around the upper steel bars, while it was only partially saturated around the lower
193 steel layer.
194



195
196 Fig. 2 Partially coated concrete beam with very low rate of oxygen transport towards the upper steel layout (test 2)

197
198 2.2 *Experimental results*

199 The output currents from each connected bar were monitored for 70 hours for both experiments.
200 The results for Test 1 (unlimited oxygen supply) and Test 2 (limited oxygen supply at the upper steel
201 layer) are presented in Fig. 3 and Fig. 4, respectively. The averaged stabilized current distribution for
202 both experiments is summarized in Fig.5 as fractions (in %) of the global protection current supplied
203 by the ZLA.

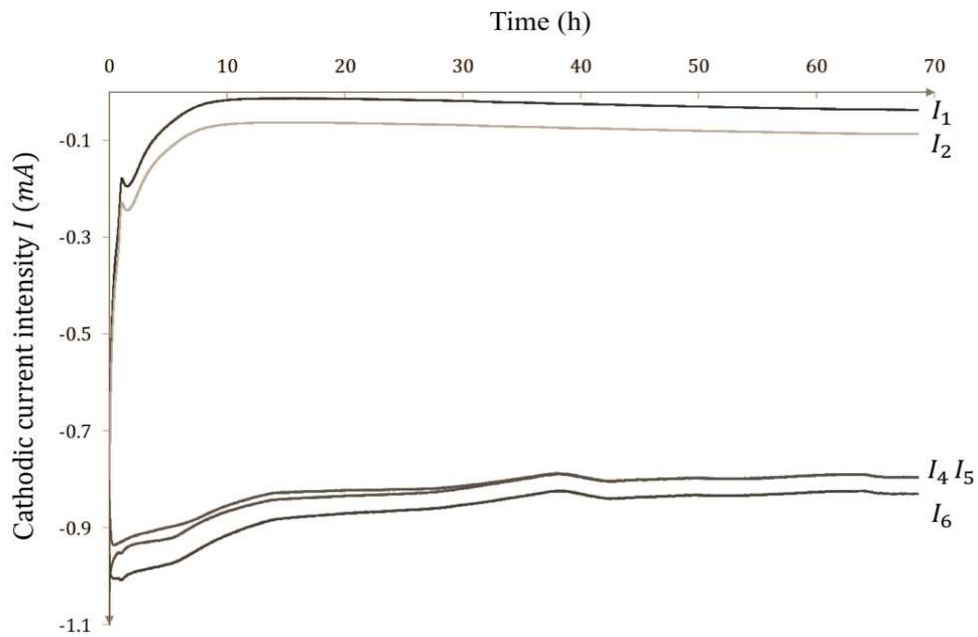


204

205

Fig. 3 Monitoring of the protection current collected by each steel bar - Test 1 (Unlimited oxygen supply)

206



207

208

Fig. 4 Monitoring of the protection current collected by each steel bar - Test 2 (Limited oxygen supply at the upper steel layer)

209

210

The global macrocell current flowing from the zinc layer anode to the reinforcing bars for unlimited oxygen supply (Test 1) was 1.8 mA , corresponding to a mean anodic current density of $47 \text{ mA} \cdot \text{m}^{-2}$ of zinc. According to Faraday's law, the rate of zinc dissolution in this specific galvanic protection system was estimated at $500 \text{ g} \cdot \text{m}^{-2} \cdot \text{year}^{-1}$.

213

214 Regarding the results of Test 1 (unlimited oxygen supply in the concrete beam), the total
215 cathodic current collected for the upper steel bars (-1.18 mA , corresponding to an averaged value of
216 $-110 \text{ mA} \cdot \text{m}^{-2}$ of steel) was almost two times that received by the lower steel bars (-0.62 mA ,
217 corresponding to an averaged value of $-39 \text{ mA} \cdot \text{m}^{-2}$ of steel) since the upper layer was closer to the
218 sacrificial anode. In this test, the ohmic resistance due to the electrical resistivity of the concrete was
219 therefore the predominant control parameter of the galvanic system. Regarding the lower layer (far
220 from the ZLA), it can be observed that the protection current collected by passive bar 6 was 30%
221 higher than the currents distributed over bars 4 and 5. This resulted from the connection asymmetry.
222 As bar 3 was unconnected, it did not receive any protection current and therefore did not induce any
223 masking effect. Another effect of the disconnection of bar 3 was observed on the upper layer steel bars,
224 where bar 2 received a significantly higher current than bar 1.

225 Nevertheless, the first important observation of this research work is that, in the conditions of
226 Test 1, the lower steel bars collected a significant amount of the total protection current provided by
227 the sacrificial anode: about 65 % of the protection current was spread over the closest bars (upper),
228 against 35 % over the lower layer. Obviously, these ratios would be slightly different if bar 3 was
229 connected in the electrochemical circuit, but it would not make the current received by the lower steel
230 bars negligible.

231 In the condition of limited oxygen supply at the upper steel layer (Test 2), the distribution of
232 the galvanic protection current was completely modified with respect to that relative to Test 1. The
233 ZLA provided a total protection current of 2.55 mA . In Fig.4, it can be clearly observed that, despite
234 their immediate vicinity to the sacrificial anode, bars 1 and 2 received very little galvanic protection
235 current (total value of -0.15 mA) while the lower layer collects a high value of protection current
236 (-2.40 mA).

237 Fig. 5 provides a quick comparison of the different current distributions observed for Test 1
238 and Test 2. The upper steel bars collected about 65 % of the galvanic current supplied by the ZLA in
239 the conditions of Test 1. Conversely, the lower steel bars collected about 95 % of the protection
240 current in the condition of Test 2.

241 The protection current density collected by the upper steel bars dropped from $-110 \text{ mA} \cdot \text{m}^{-2}$
242 of steel, in the case of unlimited oxygen access, to $-13 \text{ mA} \cdot \text{m}^{-2}$ when oxygen access was limited by
243 water saturation and epoxy coating. Conversely, the protection current received by the lower steel
244 layer became substantially higher, reaching $-150 \text{ mA} \cdot \text{m}^{-2}$ of steel while the upper steel bars were no
245 longer able to consume electrons by oxygen reduction. In that case, a redistribution of the protection
246 current was observed towards steel areas where oxygen concentration was sufficient to fuel the
247 cathodic reaction.

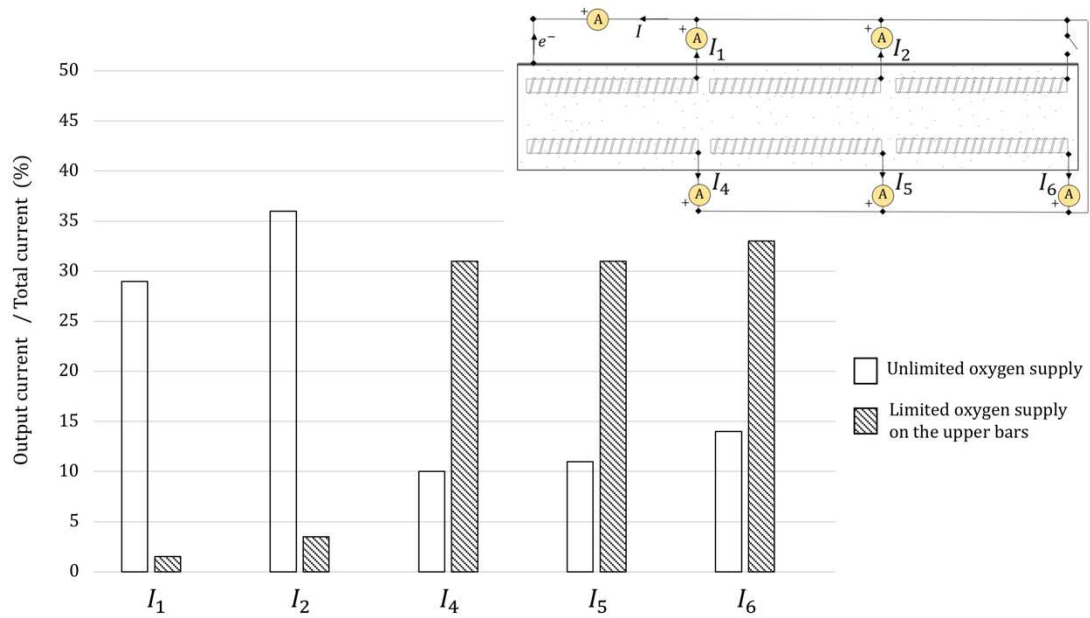
248 It has to be noted here that the global galvanic protection currents flowing from the zinc layer
249 anode to the reinforcing bars cannot be directly compared for Test 1 and Test 2 (-1.8 mA and
250 -2.55 mA , respectively) since the moisture contents of the concrete were different. The anodic current
251 produced by the zinc anode is likely to be higher in a fully saturated concrete with low electrical
252 resistivity but, at the same time, the electrical path to reach areas with high oxygen concentration was
253 longer. In these experiments, the lower global resistivity in the case of Test 2 results in a higher
254 galvanic protection current. Nevertheless, generally speaking, the global galvanic protection current
255 and its distribution over the steel reinforcements result from some balance between:

256

- The electrochemical behaviours proper to the different system components;

- 257 • Resistivity effects
- 258 • The spatial locations of the cathodic reactions (high oxygen concentration).

259 In such conditions, a relevant assessment of the galvanic protection current supplied by the
 260 sacrificial anode requires appropriate numerical simulations based on the coupling between electrical
 261 and electrochemical phenomena, and the oxygen diffusion through partly saturated concrete.



262
 263 Fig. 5 Output currents distributions for oxygen unlimited (Test 1) and oxygen limited (Test 2) oxygen supply

264

265 3 Numerical simulation approaches

266

267 This section deals with the elementary physical concepts needed to perform relevant numerical
268 simulations of the preceding experiments. Three different modelling approaches are proposed based on
269 several assumptions:

- 270 • A first modelling approach, labelled **Electrochemical model**, assumes an unlimited oxygen
271 supply at each steel-concrete interface. In such a model, the system equilibrium is controlled
272 only by resistivity effects and electrochemical behaviours (charge transfer) of the different
273 metal-concrete interfaces.
- 274 • A second approach, labelled **Diffusion model**, assumes that all the oxygen reaching steel bars
275 is consumed; here, the system equilibrium is cathodically controlled by the diffusion kinetics
276 of oxygen through concrete, i.e. by the limiting current of oxygen reduction.
- 277 • A coupled modelling approach, labelled **Multiphysics model**, addressing the interaction
278 between electrical, electrochemical and oxygen diffusion phenomena.

279 The first two approaches (Electrochemical and Diffusion models) are simplified models, but may
280 be regarded as reliable to estimate the galvanic current in some environmental conditions. Simulations
281 based on the Electrochemical model are relevant in cases of fairly dry concrete, where oxygen
282 availability is not a limiting factor. Conversely, for very wet or saturated concretes, the Diffusion
283 model may be sufficient since the galvanic equilibrium is totally controlled by the oxygen transport
284 (cathodic control). Therefore, these simplified modelling approaches should not be systematically
285 proscribed since they require significantly shorter computation time. However, for saturation degrees
286 between approximately 60 % and 90%, electrochemical effects and oxygen diffusion are in
287 competition for equilibrium control and the coupled modelling approach is necessary to achieve
288 relevant simulations.

289 In the following, numerical simulations were carried out by using the commercially-available
290 Finite Elements software Comsol Mutiphysics®. All the calculations were performed in steady state
291 conditions using the *Electric current* toolbox (EC) for electrochemical phenomena and the *Transport*
292 *of diluted species in porous media* toolbox (TDS.p) for oxygen diffusion.

293 3.1 Electrochemical model

294 At an electrochemical interface, if the charge transfer is rate limiting (no mass transport limitation), the
295 steel surface concentrations are equal to the bulk concentration. The polarization behaviour of such
296 uniform systems may be modelled by the usual Butler-Volmer equation as follows (Eq. 5) [12]:

$$297 \quad i = i_{corr} \left(\exp \left(\frac{\text{Log}(10) (E - E_{corr})}{\beta_a} \right) - \exp \left(- \frac{\text{Log}(10) (E - E_{corr})}{\beta_c} \right) \right) \quad (5)$$

297 where:

298 - i ($A \cdot m^{-2}$) is the net current density flowing through the metal-electrolyte interface of the uniform
299 corrosion system polarized at potential E (V),

300 - i_{corr} ($A \cdot m^{-2}$) is the corrosion current density at the corrosion potential E_{corr} (V),

301 - β_a and β_c ($V \cdot dec^{-1}$) are the anodic and cathodic Tafel slopes of the electrochemical system,

302 respectively.

303 The Butler-Volmer equation actually corresponds to the algebraic sum of the current densities
 304 associated with the anodic reaction of metal dissolution and the cathodic reaction of oxygen reduction.

305 The steel bars are considered as perfect electrical conductors and, thus, only the steel-concrete
 306 interface is modelled. Passive steel boundaries are modelled by the Butler-Volmer equation using an
 307 appropriate set of parameters. The electrochemical parameters involved in this work reflect the global
 308 orders of magnitude found from literature data [13]. Only the quantitative aspect of numerical results
 309 may be changed by the variability of these parameters.

310 Regarding the polarization behaviour of zinc anodes in galvanic protection, the zinc-concrete interface
 311 is almost always assumed to be non-polarizable and the zinc anode is fixed at a constant potential in
 312 numerical simulations. However, the specific electrochemical properties of ZLA have recently been
 313 measured [6], making it possible to also model the sacrificial anode as a Butler-Volmer boundary.
 314 Table 1 summarizes the electrochemical parameters involved in the following simulations and Fig. 6
 315 plots the relative polarization curves.

BV parameters	Passive steel	Zinc sheet
E_{corr} (V)	-0.1	-1.01
i_{corr} ($A \cdot m^{-2}$)	10^{-4}	$4.0 \cdot 10^{-3}$
β_a ($V \cdot dec^{-1}$)	1	0.019
β_c ($V \cdot dec^{-1}$)	0.2	0.05

Table 1 Butler-Volmer parameters used in numerical simulations.

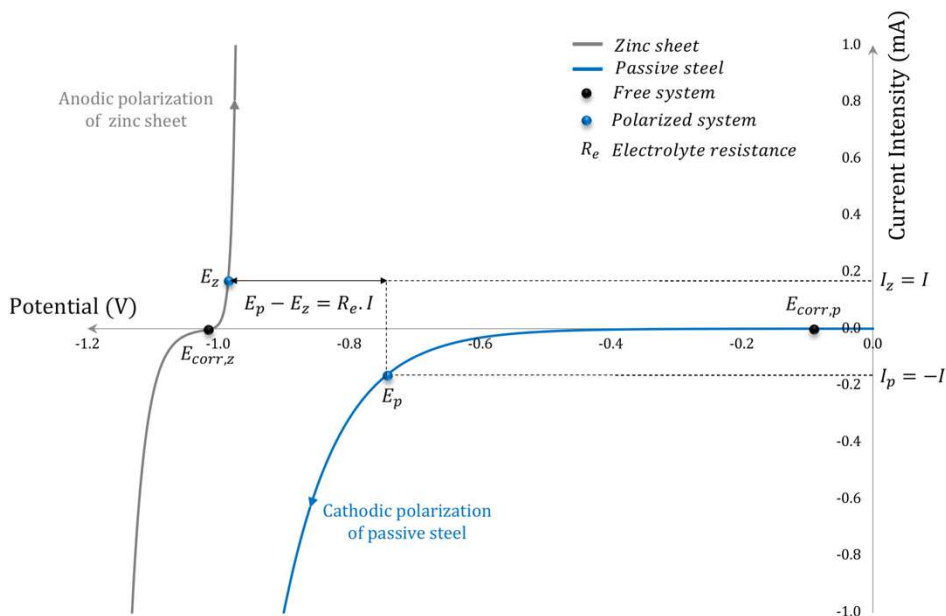


Figure 6 Qualitative electrochemical behaviours of ZLA and passive steel

322

323 In the concrete volume, the local Ohm's law (Eq. 6) and charge conservation (Eq. 7) govern electrical
324 phenomena:

$$i = -\frac{1}{\rho} \nabla E \quad (6)$$

$$\nabla \cdot i = 0 \quad (7)$$

325 where i is the local current density vector ($A \cdot m^{-2}$), E is the electric potential field (V) and ρ is the
326 electrical resistivity of concrete ($\Omega \cdot m$).

327 In order to simplify the study, the concrete is assumed to be a homogeneous, isotropic, conductive
328 material and so the electrical resistivity of concrete is considered as uniformly distributed. Therefore,
329 from Eq. 6 and Eq. 7, the potential distribution inside the concrete volume can be described by
330 Laplace's Equation (Eq. 8):

$$\nabla^2 E = 0 \quad (8)$$

331 The electrical resistivity of the concrete is a predominant parameter of the galvanic system equilibrium
332 since it strongly influences the ionic macrocell current intensity flowing from the galvanic anodes and
333 consequently the zinc dissolution kinetics. Concrete resistivity depends strongly on the volume water
334 content, w , according to a power law. Based on experimental results of the French research project
335 *SENSO* on a large range of concrete mixtures [15], the empirical relationship between water content
336 and electrical resistivity of concrete involved in this work is as follows (Eq. 9) :

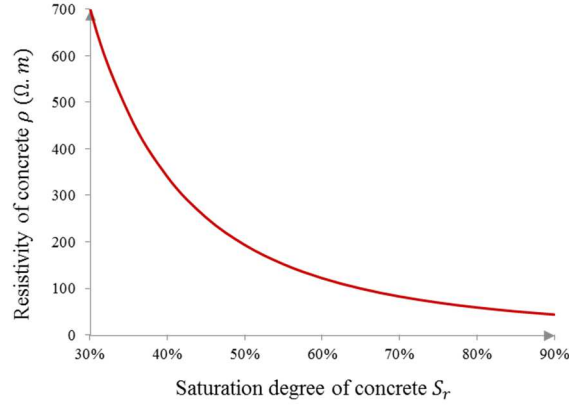
$$\rho = 0.437 w^{-2.53} \quad (9)$$

337 and:

$$w = p \cdot S_r \quad (10)$$

338 where S_r is the water saturation degree, p the porosity of the concrete and w its moisture content, all
339 these quantities being dimensionless.

340 The porosity of the concrete beam presented in section 2 was 18 %. Therefore, from Eq. 9 and Eq. 10,
341 it is possible to assess the relationship between electrical resistivity and saturation degree (Fig 7) to be
342 implemented in the following numerical simulations.



343

344

Fig. 7 Empirical relationship between electrical resistivity and saturation degree of concrete

345

The current intensity I_i (A) collected by a specific steel rod i , may be calculated by surface integration

346

of the normal cathodic current density at the steel rod-concrete interface $i_{n,i}$ ($A \cdot m^{-2}$) as follows (Eq.

347

11):

$$I_i = \iint_{S_i} i_{n,i} dS \quad (11)$$

348

The global protection current I_p is then achieved by adding the locally-collected currents I_i (Eq. 12):

$$I_p = \sum_i I_i \quad (12)$$

349

The global current can also be calculated by surface integration of the normal anodic current density

350

(I_z) produced at the zinc-concrete interface. Due to electro-neutrality, the anodic current I_z has to be

351

balanced by the cathodic current I_p as follows (Eq. 13):

$$I_z = -I_p \quad (13)$$

352

Therefore, the relative error between I_z and I_p is a measure of the convergence quality in the

353

numerical simulation.

354

The dimensions of numerical specimen were identical to those of the experimental concrete beams

355

described in section 2. The model geometry and the different boundary conditions involved in the

356

numerical simulation performed according to the Electrochemical model are illustrated in Fig. 8.

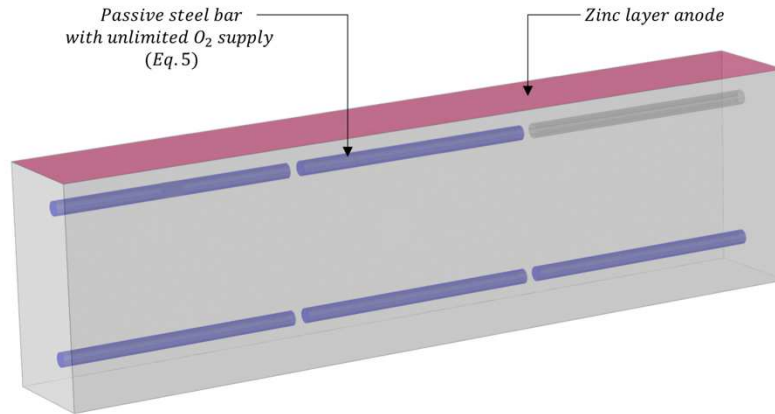


Fig. 8 Electrochemical model: geometry and boundary conditions

357

358

359

360 3.2 Diffusion model: limiting current of oxygen reduction I_{lim,O_2}

361 The diffusion model approach is based on the assumption that all the oxygen reaching any steel rod is
 362 consumed instantaneously, i.e. the oxygen concentration, c , at any steel-concrete interface is always
 363 zero. Therefore, the global cathodic current produced on the all the passive steel is limited by the
 364 oxygen diffusion kinetics in the concrete volume. Consequently, the protection current supplied by the
 365 ZLA is also controlled by oxygen diffusion since electro-neutrality has to be preserved. In this
 366 condition, the calculation of the cathodic current produced by each steel rod, which is implicitly equal
 367 to the galvanic protection current collected, may simply be deduced from the maximum oxygen flux at
 368 the steel-concrete interface. The global protection current achieved is then the global limiting current
 369 of oxygen reduction I_{lim,O_2} , which can be assessed by adding the local diffusion flows.

370 The theoretical details presented below are inspired by Aachib et al. [14], who developed a numerical
 371 approach to evaluate the oxygen flux through partly saturated media, based on experimental
 372 investigations [15].

373 Oxygen transport through the concrete cover is considered as a pure diffusion problem here, the
 374 convective part being neglected because of the assumption that water saturation of concrete is uniform
 375 and invariant. Therefore, transport of pore solution was not modelled in this study. Fick's first law,
 376 adapted to porous media, and the principle of mass conservation govern diffusion phenomena in the
 377 concrete volume, leading to the following general equation (Eq. 14):

$$p_{eff} \frac{\partial c}{\partial t} = D_e \nabla^2 c \quad (14)$$

378 where:

379 - c is the local oxygen concentration ($mol \cdot m^{-3}$),

380 - p_{eff} is the effective diffusion porosity,

381 - D_e is the effective diffusion coefficient ($m^2 \cdot s^{-1}$).

382 The effective diffusion porosity is used here to take account of both the oxygen flux in gaseous phase
 383 and the flux of oxygen dissolved in water-filled pore space (Eq. 15)

$$p_{eff} = p_a + K_H \cdot p_w \quad (15)$$

384 with

$$p_a = p \cdot (1 - S_r) \quad (16)$$

$$p_w = p \cdot S_r \quad (17)$$

385 where p_a and p_w are the volumetric air and water contents respectively, S_r is the degree of saturation,
 386 p is the concrete porosity and K_H is the dimensionless form of Henry's equilibrium constant. The latter
 387 parameter depends on temperature T ($^{\circ}C$) and atmospheric pressure p_{atm} (Pa) and may be defined by
 388 the ratio of the oxygen concentration dissolved in water c_{aq} ($mol \cdot m^{-3}$) to the oxygen concentration
 389 in air c_g ($mol \cdot m^{-3}$) as follows (Eq. 17):

$$K_H = \frac{c_{aq}}{c_g} \quad (17)$$

390 At $T = 20$ $^{\circ}C$, the oxygen concentration in air is (Eq. 18):

$$c_g = 21\% \cdot \frac{p_{atm}}{R(T + 273)} = 8.73 \text{ mol} \cdot \text{m}^{-3} \quad (18)$$

391 where R is the universal gas constant ($= 8.314 \text{ J} \cdot \text{mol}^{-1} \cdot \text{K}^{-1}$) and p_{atm} is the atmospheric pressure
 392 ($= 101325 \text{ Pa}$).

393 A typical value of K_H for oxygen at 20 $^{\circ}C$ is about 3%.

394 According to Aachib et al. [17], the semi-empirical expression of effective diffusion coefficient of
 395 oxygen D_e ($m^2 \cdot s^{-1}$) is given by (Eq. 19):

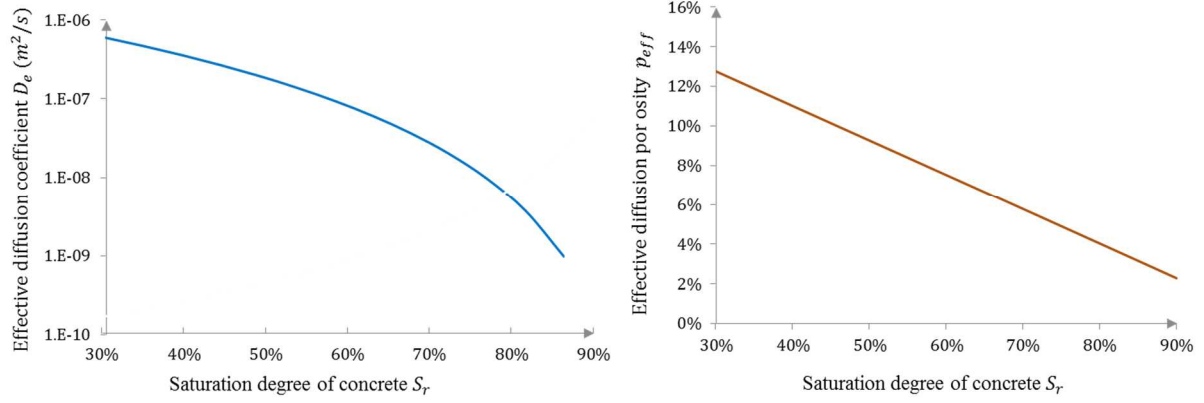
$$D_e = \frac{1}{p^2} (D_a^0 \cdot p_a^{3.3} + K_H \cdot D_w^0 \cdot p_w^{3.3}) \quad (19)$$

396 where

397 - D_a^0 is the free oxygen diffusion coefficient in air ($= 1.8 \cdot 10^{-5} \text{ m}^2 \cdot \text{s}^{-1}$),

398 - D_w^0 is the free oxygen diffusion coefficient in water ($= 2.5 \cdot 10^{-9} \text{ m}^2 \cdot \text{s}^{-1}$),

399 The concrete is considered to be uniformly saturated by water, implying uniform scalar fields of
 400 effective diffusion coefficient and effective diffusion porosity. These simulation parameters are plotted
 401 versus saturation degree in Fig. 9 for a concrete porosity of 18%.



402

403

Fig. 9 Effective diffusion coefficient (left) and effective porosity (right) plotted versus saturation degree

404

As briefly discussed above, the limiting current of oxygen reduction is the maximal value of cathodic current and may be calculated by assuming a total consumption of oxygen at the steel-concrete interface. Therefore, two types of Dirichlet boundary conditions are sufficient here to perform the simulation. They are given in Eq. 20 for the passive steel interfaces and Eq. 21 for outer, uncoated concrete surfaces exposed to air.

405

406

407

408

$$c = 0 \quad (20)$$

$$c = c_{\infty} = c_g p_{eff} \quad (21)$$

409

where c_{∞} ($mol.m^{-3}$) is the oxygen concentration in concrete on outer surfaces.

410

411

Any other boundary of the geometric model is associated with an insulation condition as follows (Eq. 22):

$$J_n = 0 \quad (22)$$

412

where J_n is the normal flux of oxygen ($mol.m^{-2}.s^{-1}$).

413

414

Then, the limiting current of oxygen reduction I_{lim,O_2} results from the surface integration of the normal oxygen flux consumed at the whole passive steel surface S_p (Eq. 23):

$$I_{lim,O_2} = \iint_{S_p} -4 F J_n dS \quad (23)$$

415

416

The limiting current I_{lim,O_2} may be compared to the cathodic current estimated with the electrochemical model I_p assuming an unlimited oxygen supply:

417

418

419

420

421

- $I_{lim,O_2} \gg I_p$: The rate of cathodic reaction is entirely controlled by charge transfer. The oxygen concentration field in the concrete volume is useless to assess the galvanic protection current here and the Electrochemical model is relevant.
- $I_{lim,O_2} \ll I_p$: The cathodic current density is entirely controlled by the rate of the mass transport and no longer depends on electrochemical processes. The potential field in the

422 concrete volume is useless to obtain the galvanic protection current here and the Diffusion
423 model is relevant.

- 424 • $I_{lim,O_2} \sim I_p$: Both the charge transfer and the mass transport determine the overall reaction rate.
425 The Multiphysics model is then necessary to perform reliable numerical simulations.

426

427 3.3 Multiphysics model

428 The Multiphysics model is built using the same constitutive equations, namely the local Ohm's law
429 (Eq. 6) and charge conservation (Eq. 7) for electrical phenomena, Butler-Volmer behaviours for
430 charge transfer phenomena, and Fick's first law adapted to porous media (Eq. 14) and mass
431 conservation for diffusion phenomena. The model coupling is performed by modifying the passive
432 steel boundary conditions slightly.

433 Oxygen molecules reaching the cathodic surfaces (passive steel rods) are reduced to hydroxide ions
434 OH^- . The time rate of OH^- ion production at passive steel surface S_p expresses the cathodic current
435 density i_c , which can therefore be easily related to the normal oxygen flux consumed at the cathodic
436 surface J_n ($mol \cdot m^{-2} \cdot s^{-1}$) as follows (Eq. 24):

$$J_n = D_e \frac{\partial c}{\partial n_{cathode}} = \frac{i_c}{-4F} \quad (24)$$

437 The Butler-Volmer equation written as Eq. 5 and used as boundary condition in the electrochemical
438 model involves an unlimited oxygen supply. As in the works by Kranc and Sagüés [16], a modified
439 Butler-Volmer equation taking the mass transport of oxygen through concrete into account is used
440 here to model steel behaviour as follows (Eq. 25):

$$i = i_{corr} \left(\exp\left(\frac{\text{Log}(10)(E - E_{corr})}{\beta_a}\right) - \frac{c}{c_\infty} \exp\left(-\frac{\text{Log}(10)(E - E_{corr})}{\beta_c}\right) \right) \quad (25)$$

441 Therefore, the problem variables E and c are coupled thanks to the passive steel boundary
442 condition. Thus, the solution of the coupled physical problem is obtained by determining:

- 443 • The concentration distribution of oxygen dissolved in the pore solution of the concrete,
- 444 • The electrical potential field and the protecting current distribution flowing in the
445 concrete volume from the galvanic anode towards the reinforcing steel bars.

446 Fig. 10 illustrates the geometry and boundary conditions for the numerical simulation based on
447 the Multiphysics model.

448

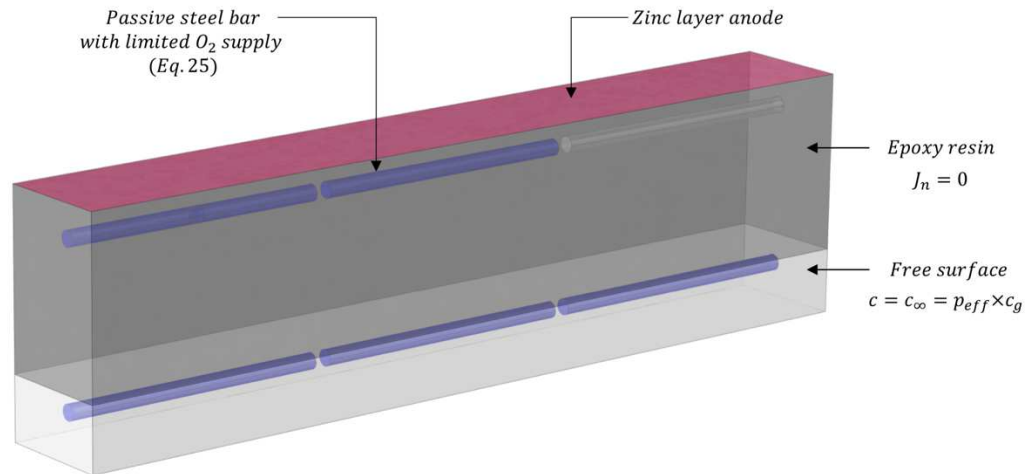


Fig. 10 Multiphysics model: geometry and boundary conditions

4 Experimental validation of the numerical results

In this section, a preliminary numerical study is carried out in order to describe the effect of the water content of concrete on the behaviour of the cathodic protection system in the case of uniform moisture saturation in the concrete volume. Then, specific simulations of the two experiments presented in section 2 are presented and discussed. The simulated cathodic currents produced by individual steel bars (i.e. the galvanic protection current received by each steel bar) are compared with experimental results to highlight the robustness and reliability of the modelling approaches.

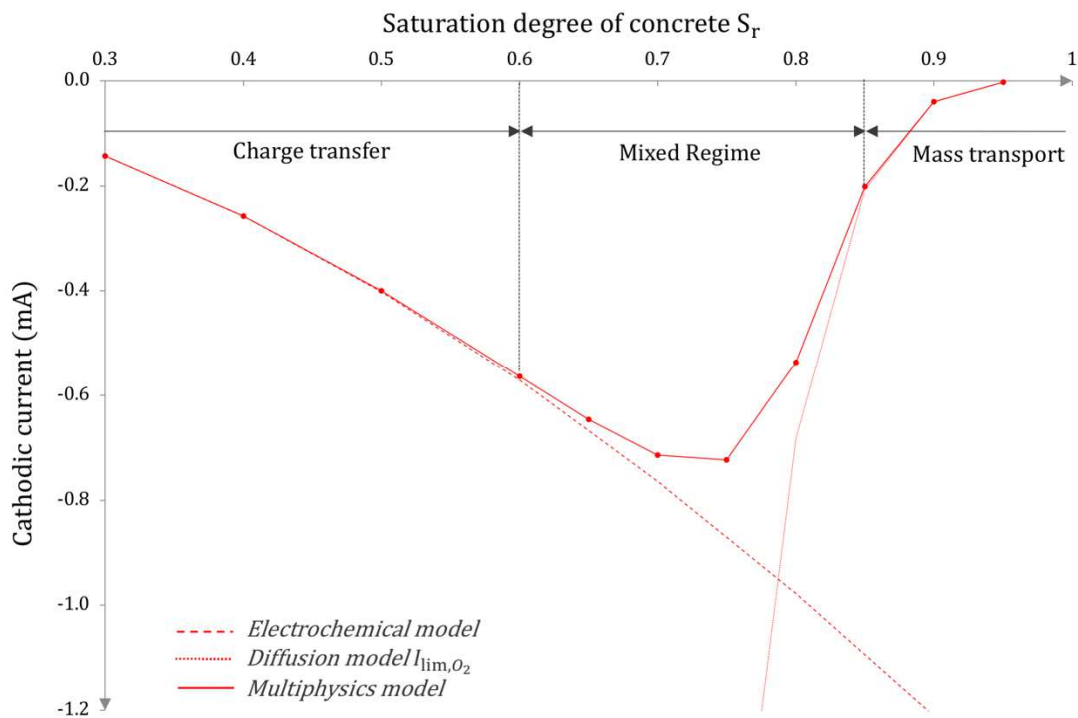
4.1 Preliminary numerical simulation of the effect of the concrete saturation degree

Here, a special attention is given to the effect of concrete water saturation on the cathodic protection current received by the steel bars in the case of uniform water distribution in the concrete volume. The numerical specimen reproduces the geometry and steel layout of the experimental beams presented in section 2. The three modelling approaches are involved here to cover the validity domains of the Electrochemical and Diffusion models. The Multiphysics model is then regarded as the only reliable numerical tool to correctly assess the galvanic protection current on the overall range of water saturation degrees.

Fig. 11 focuses on the specific current received by bar 1 (I_1), but the same qualitative results were observed for the other steel rods, giving different current magnitudes according to their respective locations in the concrete volume. The figure presents the numerical relationship between the water saturation degree and the bar current I_1 . As stated above, this current represents the kinetics of the cathodic reaction at the surface of bar 1, which is actually the fraction of the ZLA galvanic protection current it receives. For water saturation degrees of less than 60%, it is observed that the Electrochemical model is asymptotically equivalent to the Multiphysics model. For such saturation degrees, the amount of oxygen at the concrete-steel interface is the same as at the free surfaces of the concrete structure. The kinetics of the ZLA galvanic system is therefore entirely controlled by charge transfer at the metal-concrete interfaces and by the electrical resistivity of the concrete.

480 Conversely, for water saturation degrees higher than 85%, asymptotic convergence of the
 481 Diffusion and Multiphysics models is observed, meaning that the Diffusion model provides good
 482 estimation of the level of galvanic protection for wet concrete conditions. Here, the oxygen reduction
 483 is faster than its transport from the external atmosphere towards the steel bars and the electrical
 484 resistivity is so low that it is not a control parameter. Therefore, the galvanic protection process is
 485 controlled by the kinetics of oxygen diffusion through the concrete. The limiting current of oxygen
 486 diffusion is reached and the total consumption of oxygen on passive steel areas is thus a reliable
 487 boundary condition.

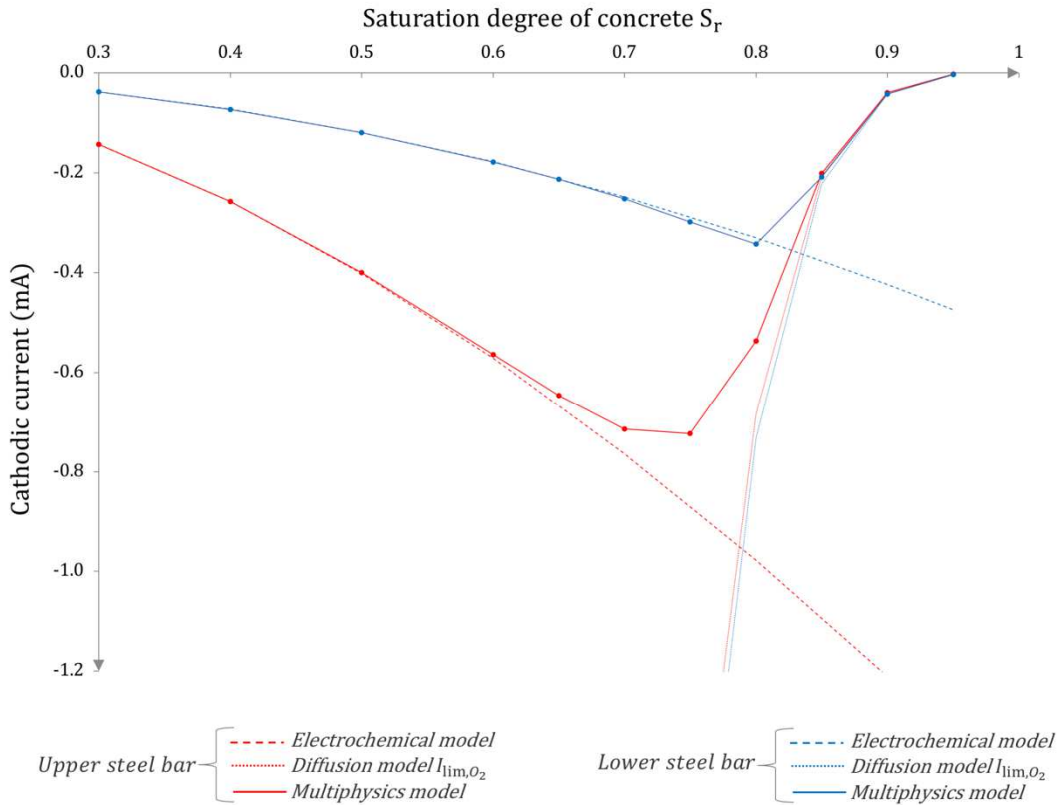
488
 489 In the 60 % to 85 % moisture saturation range (Mixed regime), both the charge transfer and the
 490 mass transport determine the overall reaction rate. The simplified assumptions involved in the
 491 Electrochemical and Diffusion models are then inaccurate, since both models lead to an
 492 overestimation of the protecting current. The existence of the Mixed regime results from the
 493 competition between oxygen diffusion and electrical resistivity for intermediate saturation degrees.
 494 This competition leads to the existence of an optimal water saturation degree for which the protecting
 495 current rate is maximal. Here, the optimal degree of water saturation is approximately 75% and the
 496 maximal protection current received by the bar 1 is found to be -0.72 mA , corresponding to an
 497 average current density of -135 mA/m^2 of steel.



498
 499 Figure 11 Numerical simulations of the protection current received by the upper-layer bar 1 (I_1) as a function of the water
 500 saturation degree of concrete (based on the Electrochemical, Diffusion and Multiphysics models)

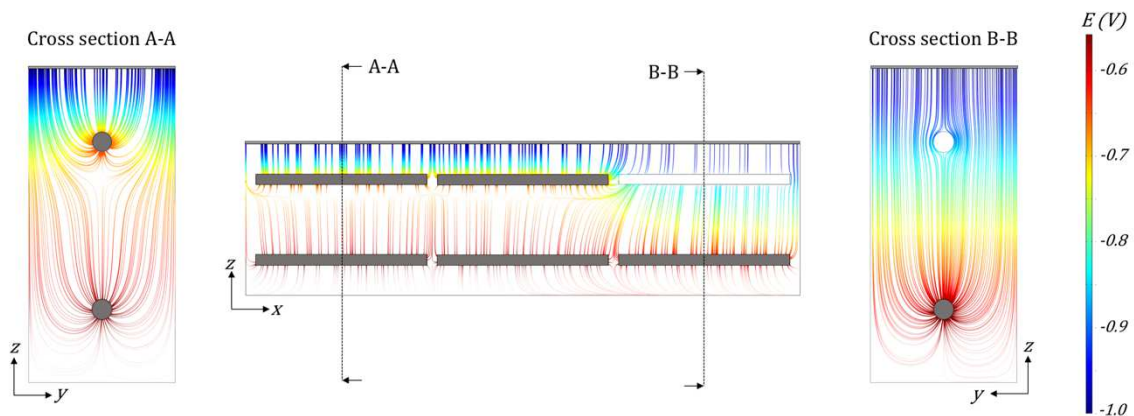
501 Due to geometrical effects, in particular the respective locations of the passive steel bars with
 502 respect to the ZLA system, the Mixed regime and the optimal saturation degree may differ
 503 significantly among the reinforcements. Fig. 12 illustrates this statement by adding the relationship
 504 between saturation degree and protection current received by bar 4 (I_4), which is located under bar 1 in
 505 the concrete beam. It can be clearly seen that the current response relative to the Electrochemical
 506 model for bar 4 (blue dashed line) is significantly lower than that of bar 1 (red dashed line). This is
 507 simply explained by the by the fact that the I_4 current streamlines encounter higher electrolytic

508 resistance (R_e) resulting from the greater electrical path length from the ZLA system at the top surface
 509 of the beam to the lower passive steel layer.
 510



511
 512 Figure 12 Numerical simulations of the protection currents received by the upper-layer bar 1 (I_1 – red lines) and the lower-
 513 layer bar 4 (I_4 – blue lines) as a function of the water saturation degree of concrete (based on the Electrochemical, Diffusion
 514 and Multiphysics models)

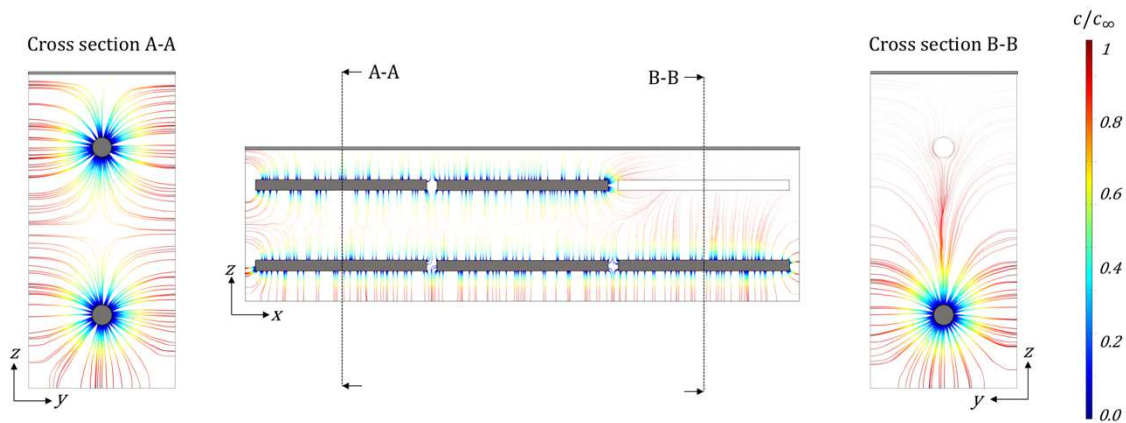
515 The global cathodic protection current streamlines are shown in Fig. 13 for a 60 % - uniform
 516 saturation degree. The cross-section A-A reveals the ZLA current distribution towards bars 1 and 4
 517 and the graphical streamline thickness and density around the bars represents the magnitude of the
 518 protection current they receive. The difference in electrical path length between ZLA to bar 1 and ZLA
 519 to bar 4 results in thicker and more dense current streamlines around bar 1, meaning a higher value for
 520 I_1 than for I_4 . In Fig.13, the cross section B-B shows that no protecting current reaches bar 3, since it
 521 was modelled as unconnected to the ZLA system, as in the experiments described in section 2.
 522



523
 524 Figure 13 Cathodic protection current streamlines and potential distribution within the concrete beam calculated with
 525 electrochemical model for a water saturation degree of concrete of 60%

526 However, at high saturation degrees, the Diffusion response of bar 4 is practically identical to
 527 that of bar 1 (Fig. 12). The similarity in these purely diffusive behaviours is explained by Fig.14,
 528 which presents the oxygen flux streamlines responsible for the effective values of oxygen-reduction
 529 limiting currents at each passive steel rod. From the diffusive point of view, the location of the ZLA
 530 with respect to a specific steel bar has no influence, since the cathodic rate is only controlled by the
 531 amount of oxygen supplied. Therefore, here, the location of the steel bar with respect to the external
 532 surface of the concrete (where oxygen is available) is the most relevant influencing factor. In Fig. 13,
 533 it is observed that oxygen comes primarily from the lateral faces of the concrete beam. Therefore, the
 534 distance between the bars and the external faces is almost identical for either the upper or the lower
 535 steel bars, meaning that the oxygen-reduction limiting currents are very similar for all the steel bars.
 536

537 From the lowered Electrochemical response of bar 4 (compared to bar 1) and its Diffusion
 538 response identical to that of bar 1, it is trivial to observe and understand that the Mixed regime region
 539 of bar 4 is shifted towards higher saturation degrees. For bar 4, the optimal saturation degree is about
 540 80 % and the associated maximum protection current is -0.3 mA .



541
 542 Figure 14 Oxygen flux streamlines and oxygen supply distribution within the concrete slab calculated with the diffusive
 543 model for a water saturation degree of concrete of 60%

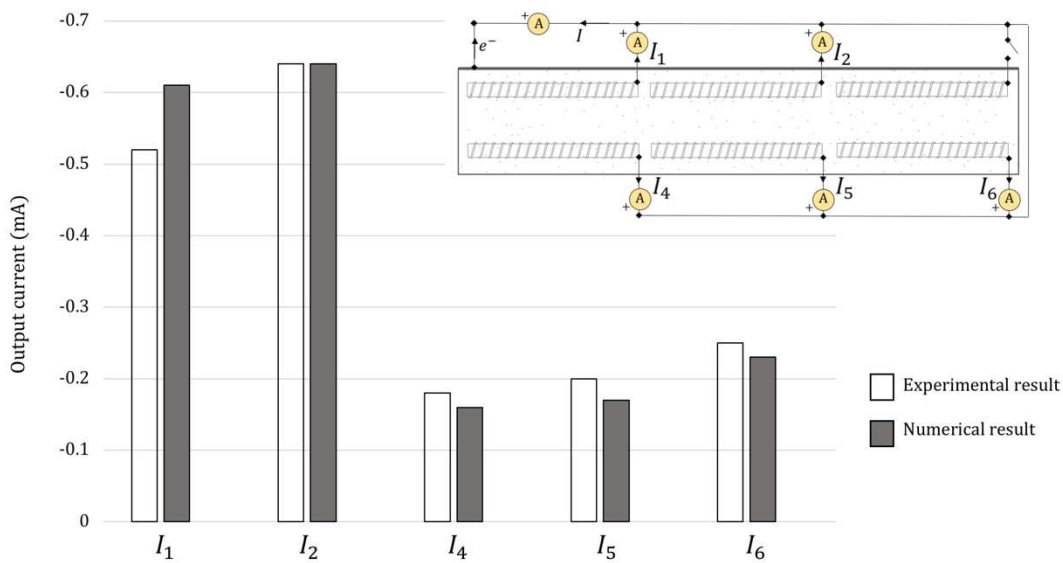
544 This preliminary numerical study highlights the difficulty of establishing global validity domains, in
 545 terms of range of saturation degree, for the Electrochemical and Diffusion models. Indeed, it has been
 546 demonstrated here that the validity domains depend on the steel bar under consideration and, in
 547 particular, its location with respect to the ZLA, but also with respect to the oxygen source. Therefore,
 548 except for very specific conditions (very dry concrete or very wet concrete), it appears hazardous to
 549 use the two simplified models for structures with complex shapes, complex steel layouts or complex
 550 boundary conditions. The decision to use one of these models requires a careful assessment of whether
 551 or not it is applicable.

552 4.2 Numerical simulation of Test1 (unlimited oxygen supply) – Electrochemical model

553 This section addresses the numerical simulation of experimental Test 1. As briefly discussed in section
 554 2, a complementary investigation revealed that a fairly uniform concrete saturation degree of 60 %
 555 was achieved in the conditions of Test 1 after a natural-drying period in the air-conditioned test room.
 556 The saturation degree was measured on small concrete cylinders coming from the same concrete batch
 557 as the experimental specimen. At this level of hydric equilibrium, the oxygen diffusion mainly occurs
 558 in the gaseous phase of the cementitious matrix, so there is no significant limitation on oxygen
 559 transport in the concrete. Taking into account the conclusions of the preliminary numerical study
 560 above, the numerical simulation of Test 1 using the Electrochemical model is relevant since the
 561 oxygen supply is considered as sufficient to fuel cathodic reactions on each steel-concrete interface.
 562

563 Fig. 15 presents a direct comparison of numerical and experimental protecting currents for
 564 each passive steel bar. It can be observed that the Electrochemical model provides a rather good
 565 estimation of the protecting current distribution over the steel rods for a uniform water saturation
 566 degree of 60 %, which corresponds well to the hydric equilibrium state of the concrete beams during
 567 the current monitoring. The simulated global macrocell current flowing from the zinc layer anode to
 568 the reinforcing bars (-1.8 mA) is in accordance with the total output current measured experimentally
 569 (-1.79 mA).

570 It is observed that the effect of the disconnection of bar 3, discussed in section 2, is also visible
 571 on the numerical simulation, as expected. Despite a numerical value of I_1 higher than the experimental
 572 one, I_2 remains higher compared to I_1 , as does as I_6 compared to I_4 and I_5 .



573

574 Fig. 15 Comparison of experimental and simulated protecting current distributions – Test 1 (unlimited oxygen supply)

575 The current and potential distributions within the concrete beam corresponding to Test 1 (60 %
 576 saturation degree) are displayed in Fig.13 using a rainbow colour range to express local potential
 577 values. As expressed above, the line thickness reflects the norm of the local current density vector i .
 578 Thin lines correspond to a low ionic current while thick lines reflect a higher current density.
 579 Qualitatively, the masking effect of the upper steel layer is illustrated by the gradual decrease of the
 580 line thickness over depth due to an increasing ohmic resistance. By comparing cross-sections A-A and
 581 B-B, it can be clearly seen that bar 6 (B-B) receives more protecting current from the ZLA than bar 4
 582 does, since the unconnected bar 3 does not produce any masking effect.

583

584

585

586

587

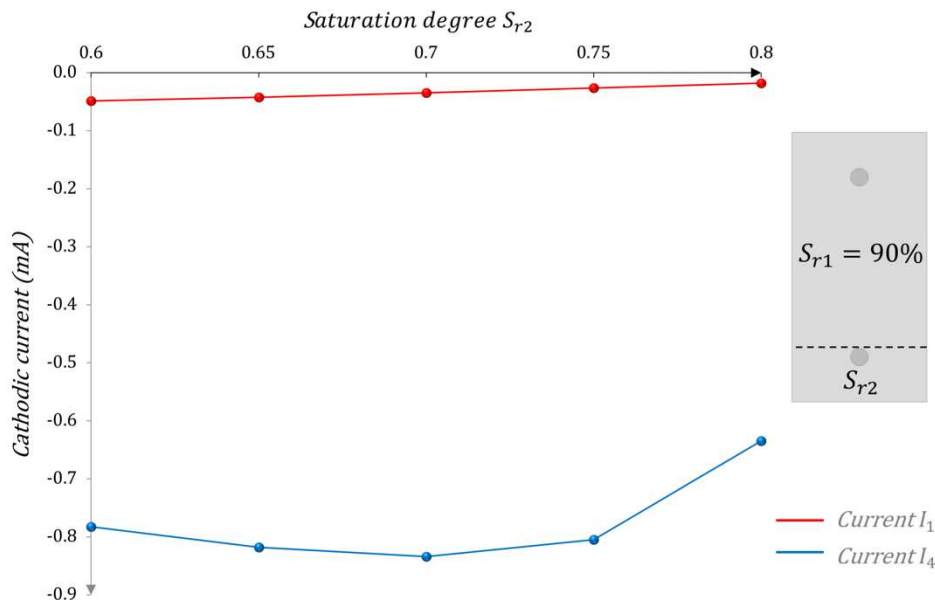
588 4.3 Numerical simulation of Test 2 (limited oxygen supply) – Multiphysics model

589 Unlike in Test 1, the moisture content of the coated concrete beam (Test 2) cannot be assessed
590 experimentally. The uncoated lower part of the specimen (below the lower steel layer) had been stored
591 out of water, leading to a partially saturated concrete. Conversely, the coated upper part of the beam
592 was close to the total water saturation since it was sealed before drying.

593 The hydric field within the concrete volume therefore has to be inferred by appropriate
594 assumptions. Nevertheless, the mass transport cannot be neglected when simulating the measured
595 output currents from the connected bars, since the oxygen supply is limited, at least in the upper
596 coated part of the specimen, and only the Multiphysics model is relevant here.

597 To infer the hydric field in the concrete volume in the conditions of Test 2, preliminary
598 numerical simulations based on the Multiphysics model were carried out (Fig.16). As a first
599 approximation, the numerical model may be considered as two distinct domains with different
600 saturation degrees. It should be noted here that the modelling of water transport through concrete is
601 outside the scope of this study. The concrete in the upper, coated, part of the specimen is assumed to
602 have a uniform degree of saturation, labelled S_{r1} , and the concrete in the lower, uncoated, part is
603 associated with a different saturation degree, labelled S_{r2} . The saturation degree of the coated part
604 S_{r1} was inferred to be 90 %, which is a realistic value for saturated concretes and an accurate
605 assumption. Then, a series of numerical simulations were performed by varying the saturation degree,
606 S_{r2} , of the lower part, which is more difficult to assess reliably. The variation range of S_{r2} involved in
607 the simulations was between 60 and 80 %. The simulation results are displayed in Fig.16 as the
608 numerical relationship between the protection currents received by bars 1 and 4 and the saturation
609 degree of the lower, uncoated, concrete volume, S_{r2} .

610



611

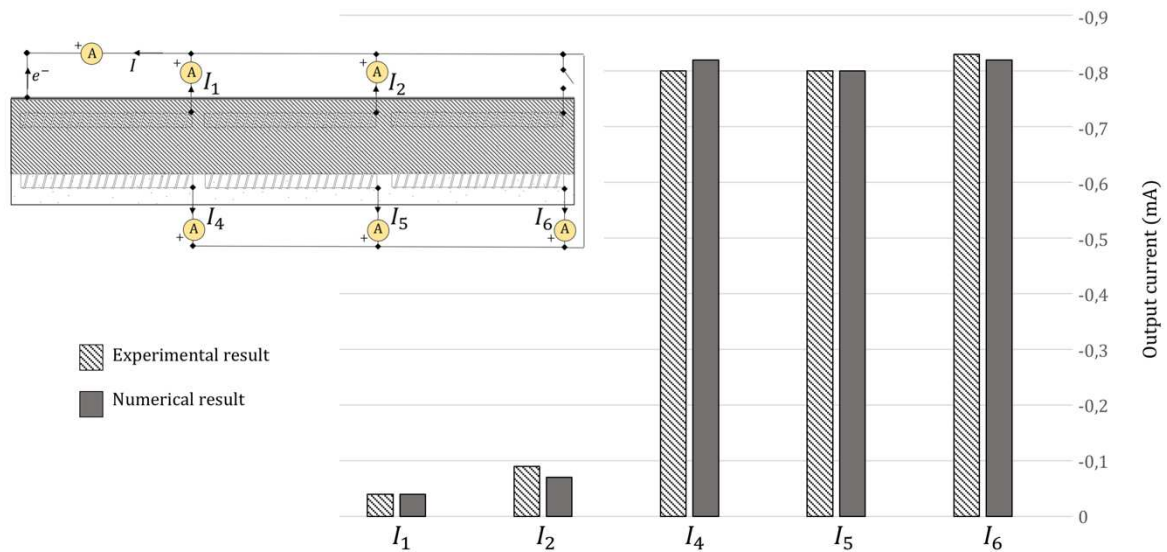
612 Fig. 16 Simulated output currents I_1 (in red) and I_4 (in blue) as a function of the saturation degree S_{r2} within coated concrete
613 beam

614 As observed in the experiment of Test 2, the numerical simulations show a significantly higher
615 cathodic current for bar 4 than for bar 1. More generally, a higher fraction of the galvanic protection

616 current appears to be collected by the lower steel bars due to the very low amount of oxygen in the
 617 upper part of the concrete. The robustness of the Multiphysics modelling approach is highlighted here
 618 since it is able to reproduce experimental data. For saturation degrees S_{r2} lying between 60 and 75 %,
 619 the current received by bar 4 is stabilized at around -0.8 mA , meaning that charge transfer controls
 620 the cathodic reaction in such a saturation range of the lower concrete part. At higher saturation degrees
 621 ($S_{r2} = 80 \%$), the protection current is lowered by about 20 %, meaning that oxygen access in the
 622 lower concrete part is more difficult. Regarding the behaviour of bar 1, the very low cathodic current
 623 is linearly lowered with the increase in S_{r2} . This relationships results from the fact that, even for the
 624 upper steel bar, the very low amount of oxygen available for cathodic reaction comes from the lower
 625 part of the beam in such a testing condition.

626 Regarding the relative stability of the protection current in the S_{r2} saturation range from 60 to
 627 75 %, the mid-range value of 67.5 % was chosen to infer the saturation degree of the lower concrete
 628 volume in the conditions of Test 2. Due to this stability, the possible error with respect to the effective
 629 saturation range produced only very slight deviations in the simulated currents.

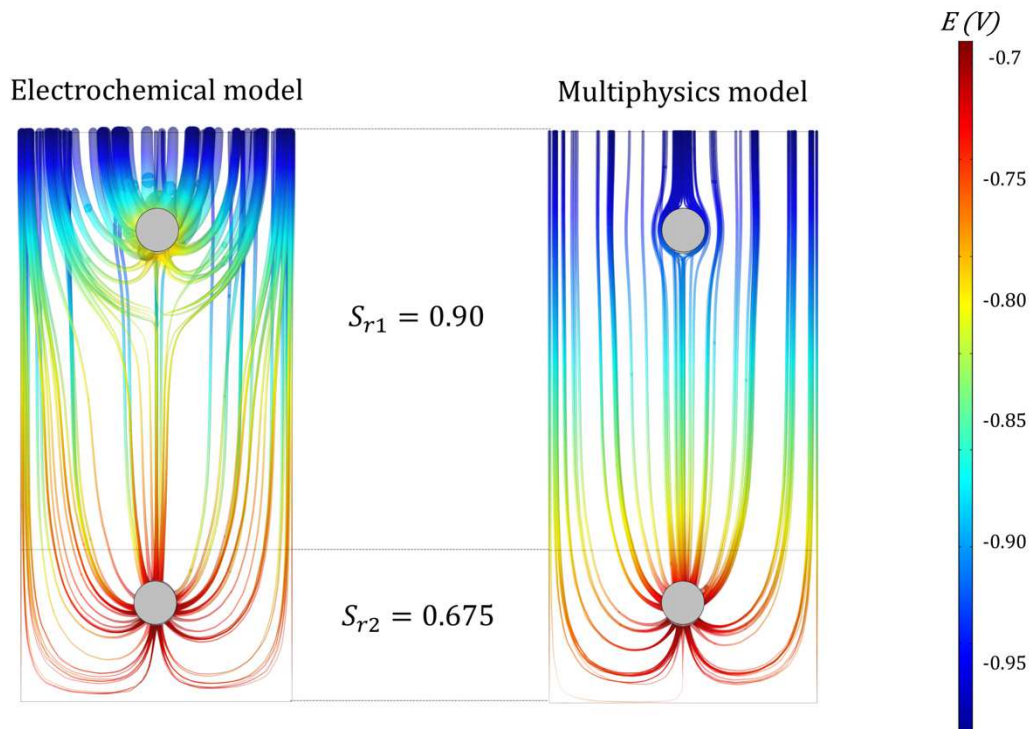
630 Fig.17 presents a direct comparison of numerical and experimental protecting currents for each
 631 passive steel bar in the conditions of Test 2. The experimental current distribution appears almost
 632 identical to the numerical one, estimated with the Multiphysics model for the following hydric field:
 633 $S_{r1} = 90 \%$ and $S_{r2} = 67.5 \%$. The global macrocell current flowing from the zinc layer anode to the
 634 steel network is, moreover, found to be equal to the galvanic current measured experimentally
 635 (-2.55 mA).



636

637 Fig. 17 Comparison of experimental and simulated protecting current distributions – Test 2 (limited oxygen supply at the
 638 upper steel layer)

639 The Multiphysics model appears relevant and robust here to describe physical phenomena
 640 occurring in the conditions of Test 2. Neglecting the effect of oxygen transport, by implementing a
 641 pure Electrochemical model, would lead to considerable error in such a case. In order to confirm this
 642 statement, Fig.18 compares current distributions from the ZLA to the steel bars, achieved by the
 643 Electrochemical model (left) and by the Multiphysics model (right) in the conditions of Test 2.



644

645 Fig. 18 Comparison of the numerical protection current streamlines and local potential fields within the coated concrete beam
 646 (cross section A-A) based on Electrochemical (left) and Multiphysics (right) models for a hydric field of 90% in the upper
 647 part of the specimen and 67.5 % in the lower part.
 648

649 By considering charge transfer and concrete electrical resistivity as the only limiting factors in
 650 the Electrochemical simulation (left), the protection current is distributed in a very different way from
 651 that achieved with the multiphysics interaction between the electrochemical process and oxygen
 652 diffusion (right). In such environmental conditions, the Electrochemical model leads to a significantly
 653 higher fraction of the protection current collected by the upper steel layer, which was experimentally
 654 demonstrated to be irrelevant. The Electrochemical model is clearly not suitable here, since the mass
 655 transport, as well as the charge transfer and the concrete resistivity, determine the overall reaction rate.

656

657 5 Conclusion

658

659 This paper addresses the spatial distribution of the galvanic protection current provided by a Zinc
 660 Layer Anode system (ZLA) over a reinforcing steel network embedded in a concrete beam. Two
 661 specific cases are studied: unlimited and limited oxygen supply to the steel bars. The results of original
 662 experiments carried out to assess the current distribution in the concrete specimen are discussed for
 663 both oxygen-supply conditions. The theoretical details of three possible modelling approaches are then
 664 presented. Finally, numerical simulations of the experiments are reported and discussed. The findings
 665 of this research work provide original insight into the physical complexity relative to the galvanic
 666 protection of reinforcing steel in concrete and show that the classical design approach of such
 667 protecting systems should be reconsidered.

668 Despite a few research works in the literature on the interaction between electrochemical processes
669 and oxygen diffusion, the electrical resistivity is still considered as the predominant control parameter
670 of a galvanic protection system. This statement is implicitly the reason why only the steel bars close to
671 the anodic system are usually considered by designers as being concerned in the galvanic exchange. In
672 this paper, it is demonstrated that the oxygen transport can be neglected only in the case of a dry
673 concrete. Moreover, in some specific, but realistic and possibly quite frequent, conditions, distant steel
674 bars may collect more protecting current than steel bars close to the anodic system.

675 Actually, the global system equilibrium, i.e. the natural macrocell current supplied by the ZLA and its
676 spread over the whole steel network in the concrete volume, results from some predominant
677 influencing factors:

- 678 • The geometry of the reinforced concrete element, including the steel layout;
- 679 • The field of electrical conductivity of the concrete;
- 680 • The charge transfer processes at the metal-concrete interfaces;
- 681 • The oxygen supply to the steel bar.

682 By considering the last three influencing factors mentioned above, it is trivial to deduce that the
683 volumetric water content of the concrete is a key issue since an increase in the water saturation degree
684 leads simultaneously to:

- 685 • An increase in the electrical conductivity and therefore in the charge transfer kinetics, which
686 tend to increase the global galvanic protection current exchanged between the ZLA system
687 and the steel network;
- 688 • A decrease in the oxygen supply to the cathodic areas, which tends to decrease the galvanic
689 protection current.

690 Consequently, for varying water saturation degrees of the concrete, the galvanic protection system
691 equilibrium is determined by the competition between the charge transfer processes and the oxygen
692 transport through the concrete. Due to these opposite effects of moisture content on oxygen diffusivity
693 and charge transfer (related to electrical conductivity of the concrete), an optimal water saturation
694 degree exists, for which the macrocell current produced by the zinc layer anode is maximal. Moreover,
695 taking account of the possible non-uniformity in the concrete water saturation, the steel layer
696 immediately next to the sacrificial anode does not systematically collect the highest fraction of the
697 protecting current. One of the experiments presented in the paper clearly demonstrates that distant
698 steel bars may collect much more protection current than the ones close to the ZLA, providing some
699 specific conditions hold for oxygen distribution in the concrete volume.

700 Nevertheless, such conditions can occur in real structures, especially in the case of ZLA galvanic
701 protection, for which the oxygen supply towards the shallow steel bars may be limited, or even
702 avoided by the ZLA sheet itself. The galvanic protection current is then spread over more distant steel
703 bars where the oxygen amount is sufficient to fuel the cathodic reaction. So, when designing such
704 galvanic protecting systems, considering only the closest steel bars (with respect to the anodic system)
705 is likely to lead to erroneous predictions of the cathodic protection efficiency.

706 Regarding the physical complexity related to the effective distribution of the protection current on the
707 whole steel network, it appears that the design of cathodic protection systems by using unjustified
708 assumptions and simple analytical rules may lead to inconsistent solutions. Due to the real 3D nature
709 of the problem, only appropriate numerical simulations based on robust models can provide some
710 physical justifications to the design of a specific cathodic protection system adapted to a specific

711 reinforced concrete element, with its own environmental conditions, its own geometry... The
712 qualitative and quantitative agreement between experimental and numerical results presented in this
713 paper shows that robust and parsimonious modelling approaches are available to improve the cathodic
714 protection design.

715 Further scientific developments are currently underway to improve these modelling approaches by
716 taking account of the water transport within the pore network, in order to implement non-uniform
717 fields of water saturation rather than uniform fields applied over the whole concrete volume. Moreover,
718 the seasonal variations in the structure environmental conditions imply that the galvanic equilibrium
719 should be addressed as a time dependent problem, with a time-varying protection current value and
720 distribution.

721

722 References

- 723 [1] R. Francois, "Effect of damage in reinforced concrete on carbonation or chloride penetration,"
724 *Cem. Concr. Res.*, no. 9, 1988.
- 725 [2] "NACE International, CP - 2 Cathodic Protection Technician Course Manual, Nace, Houston
726 2000," vol. 49, no. 2, pp. 80–102, 2000.
- 727 [3] "ISO 12696:2016 Cathodic protection of steel in concrete," no. 122457, 2016.
- 728 [4] S. Laurens, P. Hénocq, N. Rouleau, F. Deby, E. Samson, J. Marchand, and B. Bissonnette,
729 "Steady-state polarization response of chloride-induced macrocell corrosion systems in steel
730 reinforced concrete - Numerical and experimental investigations," *Cem. Concr. Res.*, vol. 79,
731 pp. 272–290, 2016.
- 732 [5] A. Clément, S. Laurens, G. Arliguie, and D. Deby, "Numerical study of the linear polarization
733 resistance technique applied to reinforced concrete for corrosion assessment," *Eur. J. Environ.
734 Civ. Eng.*, 2012.
- 735 [6] D. Garcia, S. Laurens, and S. Panin, "Electrochemical behavior of zinc layer anodes used for
736 galvanic protection of steel in reinforced concrete," *RILEM Tech. Lett.*, vol. 3, pp. 59–65, 2018.
- 737 [7] M. Raupach, "Investigations on the influence of oxygen on corrosion of steel in concrete—Part
738 2," *Mater. Struct.*, vol. 29, no. 4, pp. 226–232, 1996.
- 739 [8] B. Huet, V. L'hostis, G. Santarini, D. Feron, and H. Idrissi, "Steel corrosion in concrete:
740 Determinist modeling of cathodic reaction as a function of water saturation degree," *Corros.
741 Sci.*, vol. 49, no. 4, pp. 1918–1932, 2007.
- 742 [9] L. Bertolini and E. Redaelli, "Throwing power of cathodic prevention applied by means of
743 sacrificial anodes to partially submerged marine reinforced concrete piles: Results of numerical
744 simulations," *Corros. Sci.*, vol. 51, no. 9, pp. 2218–2230, 2009.
- 745 [10] M. M. S. Cheung and C. Cao, "Application of cathodic protection for controlling macrocell
746 corrosion in chloride contaminated RC structures," *Constr. Build. Mater.*, vol. 45, pp. 199–207,
747 2013.
- 748 [11] J. Ožbolt, G. Balabanić, and M. Kušter, "3D Numerical modelling of steel corrosion in
749 concrete structures," *Corros. Sci.*, vol. 53, no. 12, pp. 4166–4177, 2011.
- 750 [12] J. Warkus, M. Raupach, and J. Gutikers, "Numerical modelling of corrosion - Theoretical

- 751 backgrounds,” *Mater. Corros.*, vol. 57, no. 8, pp. 614–617, 2006.
- 752 [13] J. Gulikers and M. Raupach, “Numerical models for the propagation period of reinforcement
753 corrosion: Comparison of a case study calculated by different researchers,” *Mater. Corros.*, vol.
754 57, no. 8, pp. 618–627, 2006.
- 755 [14] M. Aachib, M. Mbonimpa, and M. Aubertin, “Measurement and Predictions of the Oxygen
756 Diffusion Coefficient in Unsaturated Media, With Applications to Soil Covers,” *Water. Air.
757 Soil Pollut.*, vol. 156, pp. 163–193, 2004.
- 758 [15] R. Millington and R. Shearer, “DIFFUSION IN AGGREGATED POROUS MEDIA.,” *Soil
759 Sci.*, 1971.
- 760 [16] S.C. Kranc and A.A. Sagüés, “Electrochemical impedance of corrosion macrocells on
761 reinforcing steel in concrete,” *Corros. 90*, vol. Paper N#13, pp. 1355–1372, 1990.
- 762